Published in the Proceedings of the 16th International Aluminum Alloys Conference (ICAA16) 2018
ISBN: 978-1-926872-41-4
by the Canadian Institute of Mining, Metallurgy & Petroleum

CHARACTERIZATION OF ALUMINIUM ALLOY SHEETS ACCUMULATIVE ROLL-BONDED AT DIFFERENT TEMPERATURES

*M. Karlík[1,2], P. Homola[1,3], and M. Slámová[4]

[1]Czech Technical University in Prague, Faculty of Nuclear Sciences and Physical Engineering, Department of Materials, Trojanova 13, 120 00 Praha 2, Czech Republic
*(*Corresponding author: Miroslav.Karlik@fjfi.cvut.cz)*

[2]Charles University, Department of Physics of Materials, Ke Karlovu 5, 121 16 Prague 2, Czech Republic

[3]Czech Aerospace Research Centre, Beranových 130, 199 05 Praha – Letňany, Czech Republic

[4]Research Institute of Metals, Panenské Břežany, 250 70 Odolena Voda, Czech Republic

ABSTRACT

Aluminum sheets (AA1199, AA8006, and AA5754) were processed by accumulative roll-bonding (ARB) in the temperature range from 20 to 350°C. The microstructure of the sheets was characterized by means of scanning and transmission electron microscopy and electron backscattered diffraction. Mechanical properties were monitored by hardness measurements and tensile tests. Increasing strain (number of ARB cycles) led to incremental development of lamellar microstructure with a decrease of the spacing between high-angle grain boundaries in the normal direction of sheets. ARB process produced an important increase of strength while maintaining thickness and relatively high ductility, without accenting of the anisotropy of mechanical properties of sheets. The level of hardening decreased with the processing temperature and at 300 and 350°C ARB caused even the softening of the material due to the recovery of the deformed microstructure or partial recrystallization during heating to ARB processing temperature.

KEYWORDS

Accumulative roll-bonding, AA1199, AA8006, AA5754, Electron backscatter diffraction, Hardness, Tensile testing

INTRODUCTION

Accumulative Roll Bonding (ARB) is a technique of grain refinement by severe plastic deformation (SPD) proposed by Saito et al. (1999). One ARB cycle consists in sheet cutting, surface treatment, stacking of two pieces, heating (optional), and rolling with 50% reduction in thickness. Since the sheet thickness remains unchanged by this cycle, ARB processing can be repeated as many times as desired. The goal of ARB is to impose an extremely high plastic strain on the material, resulting in structural refinement and strength increase without changing specimen dimensions. After several cycles, ultra-fine grained (UFG) materials with high strength and relatively high ductility are produced. An advantage of this method is that it does not require any special equipment as other SPD methods such as equal channel angular pressing (ECAP) (Valiev & Langdon, 2006), high pressure torsion (HPT) (Valiev et al., 2000), or cyclic extrusion and compression (CEC) (Richert et al., 1999), but only a conventional rolling mill and so it is seen as an economically viable and industrially scalable processing route. ARB processing has been successfully applied to various kinds of metallic materials at room or elevated temperatures (Tsuji, 2005). Besides processing single metals and alloys, ARB has also been used for creating ultra-fine grained and nanograined metallic composites (Wu et al., 2010; Qu et al., 2014).

Ingot cast aluminium alloys are often used as starting materials for ARB (Kim *et al.*, 2005; Roy *et al.*, 2011; Xie *et al.*, 2016). An energy efficient technology of twin-roll casting (TRC) is known to produce materials with fine particles and small grain size, which are good starting materials to further grain refinement by ARB processing. The present paper reports a comparative study of microstructure and mechanical properties of ingot cast pure aluminum (AA1199) and twin-roll cast Al-Fe-Mn-Si (AA8006) and Al-Mg (AA5754) alloy sheets ARB processed at ambient and elevated temperatures (200, 250, 300 and 350°C).

EXPERIMENTAL

A hot rolled 9.0 mm plate of AA1199 (Al99.99 wt.%) was cold rolled to the thickness of 2.0 mm. Fully recrystallized sheet was prepared by annealing for 30 minutes at 350°C. Recrystallized commercial twin-roll cast (TRC) AA8006 and AA5754 sheets (Table 1) 2.0 mm in thickness were prepared by cold rolling and annealing 450°C/30 min and 400°C/10 min, respectively. AA8006 specimens were prepared from a homogenized sheet, i.e., very low concentration of solute atoms is typical for the matrix of the material. On the other hand, the AA5754 sheet was cold rolled directly from the as-cast strip and it was only shortly annealed. Thus, the concentration of dissolved atoms in this alloy is much higher due to high-supersaturation of the solid solution during TRC.

Table 1. Chemical composition of studied materials (wt.%)

Alloy	Mn	Si	Fe	Cu	Mg	Zn	Ti	Al
AA1199 (Al99.99)	-	0.003	0.003	0.001	-	-	-	99.99
AA8006 (AlFeMn)	0.40	0.16	1.51	0.006	0.003	0.012	0.014	balance
AA5754 (AlMg3)	0.38	0.20	0.24	0.005	2.69	0.02	0.05	balance

The grain structure and intermetallic particles of studied materials in the initial condition are presented in EBSD orientation maps and SEM backscattered electron micrographs in Figure 1. The grain size of high purity aluminum, AA1199 (Figure 1a) is relatively coarse and inhomogeneous, because the microstructure of the sheet does not contain any particles nor foreign atoms in solid solution to hinder the motion of grain boundaries during annealing. On the other hand, final annealing of AA8006 and AA5754 alloys led to a recrystallized microstructure with small equiaxed grains (Figure 1b,c). In the microstructure of the AA8006 alloy there are numerous and uniformly distributed particles of intermetallic phases $Al_6(Fe,Mn)$ and α-Al(Fe,Mn)Si (Figure 1d). In the AA5754 alloy there are mainly particles of complex AlFeMn phases assembled in clusters of various shapes (Figure 1e), coarse $MgSi_2$ particles were sporadically also found.

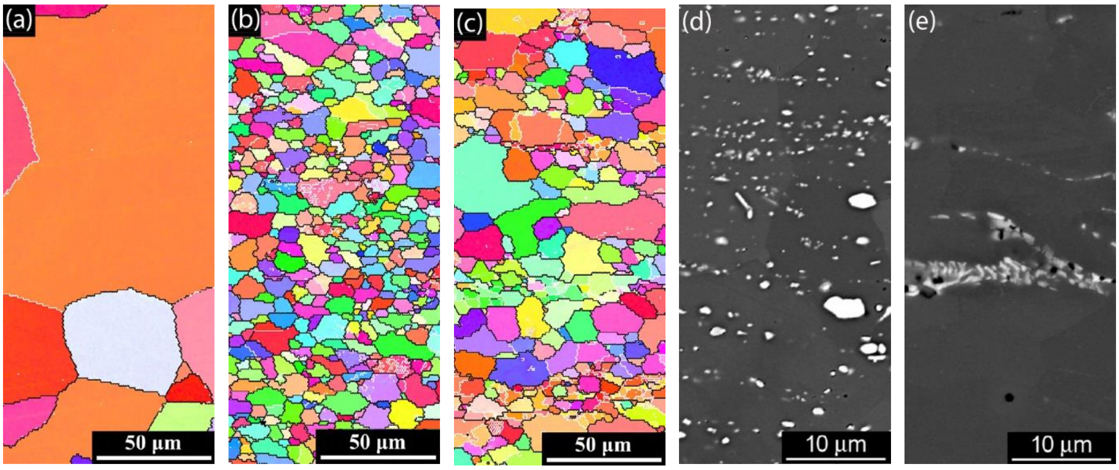

Figure 1. Grain structure of initial materials: (a) AA1199, (b) AA8006, (c) AA5754 and corresponding distribution of intermetallic phases in backscattered electron signal after etching by HF solution: (d) AA8006, (e) AA5754; the small dark features in Figures 1d,e are holes related to etched out precipitates

ARB processing consisted in the repetition of the following steps: 1) degreasing and wire-brushing with 0.3 mm steel wire brush; 2) stacking of two pieces of 300×50×2 mm^3; 3) joining by Al wires; 4) heating in furnace to 200, 250, 300 or 350°C (optional); 5) rolling without lubricant to 50% reduction in thickness. Roll diameter of 340 mm and peripheral speed of 30 m/min was used for all materials. In order to prevent the propagation of edge cracks, specimen edges were trimmed and smoothed down.

The evolution of the sheet microstructure was studied by scanning electron microscopy (SEM) electron backscatter diffraction (EBSD) orientation maps and transmission electron microscopy (TEM) on the long transverse (LT) plane. Specimens for TEM cross-sectional observations were prepared by electrolytic twin-jet polishing in 30% HNO_3 solution in methanol (pure Al) and 6% solution of $HClO_4$ in methanol (Al alloys). Hardness measurements HV10 and tensile tests on samples with 20 mm gauge length and 8 mm width served for the estimation of the evolution of strength.

RESULTS AND DISCUSSION

Evolution of the Microstructure during ARB at 20°C

EBSD maps in Figure 2 show the evolution of the grain structure of all three materials. After the first ARB cycle, inside the grains there are numerous low-angle grain boundaries (LAGB) delimiting cells and subgrains (Figure 2a,d,j). With increasing strain due to higher number of ARB cycles high-angle grain boundaries (HAGB) reorient to the direction of rolling and a lamellar grain structure is formed (Figure 2b,f,l). With increasing number of ARB cycles, the distance of HAGB in the normal direction (ND) decreases (Table 2) and this distance approaches to the size of subgrains. Simultaneously, the size of the grains in the rolling direction decreases due to their sectioning by boundaries in the ND (Figure 2h). In the AA1199 alloy, the fragmentation of deformed grains is not pronounced. Even after 6 ARB cycles there are relatively long grains still present in the microstructure (Figure 2c). Incomplete fragmentation is due to the absence of second phase particle able to pin the boundaries. In consequence, the transformation of LAGB to HAGB is restricted by dynamic recovery. On the other hand, in the AA8006 alloy, containing finely dispersed intermetallic particles, a lamellar grain structure is developed already after 3 ARB cycles (Figure 2f) and the following ARB processing leads to the fragmentation of grains and their refinement (Figure 2g–i). Even if the AA5754 alloy was ARB processed up to 5 cycles, the evolution of the grain structure by EBSD was possible only up to 3 cycles. On the samples subjected to 4 and 5 cycles ARB it was not possible to evaluate the diffraction pattern of Kikuchi lines, which was very faint, diffuse or composed by superposition of several diffraction patterns of neighboring very fine grains. Nevertheless, similarly to other materials, also in the AA5754 alloy there are cells and subgrains forming deformation bands after the first ARB cycle (Figure 2k) and the following ARB cycles lead to the formation of a lamellar grain structure with an important decrease of the distance of HAGB in the ND (Figure 2l). Figure 2j represents initial grain structure of the AA5754 alloy which was already shown in Figure 1c.

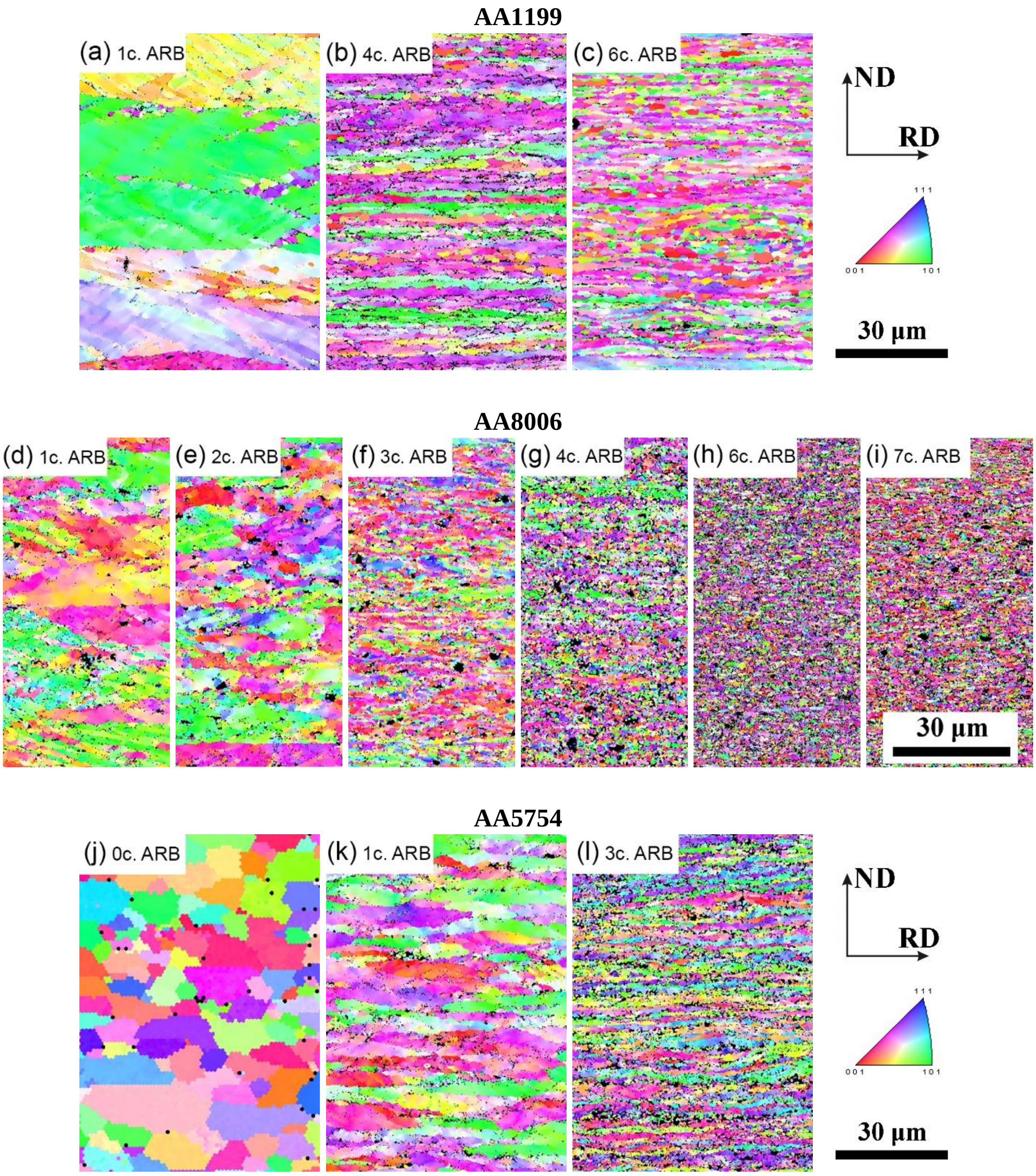

Figure 2. Orientation maps showing the evolution of the grain structure in AA1199, AA8006 and AA5754 during ARB at 20°C

Table 2. Reduction of grain size in the ND during ARB at 20°C (μm) (EBSD data, *TEM)

Alloy / ARB cycles	0	1	2	3	4	5	6	7
AA1199 (Al99.99)	53.2	2.75	1.60	1.00	0.69	0.87	0.69	-
AA8006 (AlFeMn)	7.8	1.64	1.56	0.60	0.50	0.39	0.28	0.30
AA5754 (AlMg3)	4.3	0.59	0.43	0.23	0.10*	-	-	-

Transformation of LAGB to HAGB with increasing strain is evident from the plots in Figure 3 indicating quantified results from another representation of EBSD orientation maps in Figure 2. In this representation of EBSD grain boundary maps (not shown here), the boundaries are marked by different colors according to three ranges of mutual misorientation angles of adjacent grains in three categories: i) LAGB 2 to 5°, LAGB 5 to 15°, and HAGB > 15° and then treated by image analysis. From Figure 3a it follows that for AA1199 in the initial condition, completely softened by annealing, more than 2/3 of grain boundaries are HAGB. During the first two ARB cycles, many LAGB are formed and their percentage rises up to 77.4%. The fraction of HAGB and LAGB remains practically constant up to two ARB cycles and starting from the third one, the percentage of HAGB uniformly increases up to 57.8% after 6 cycles. While the behavior of the AA8006 alloy with finely dispersed intermetallic particles in the microstructure is similar in the first two ARB cycles (Figure 3a), already during the 3rd cycle the fraction of HAGB increases to 63.2% and it rises further up to 83.5% after 7 ARB cycles (Figure 3b). In the AA5754 alloy, the course of HAGB and LAGB percentage is similar (Figure 3c), but the fraction of LAGB (2°-5°) is higher at the expense of LAGB (5–15°).

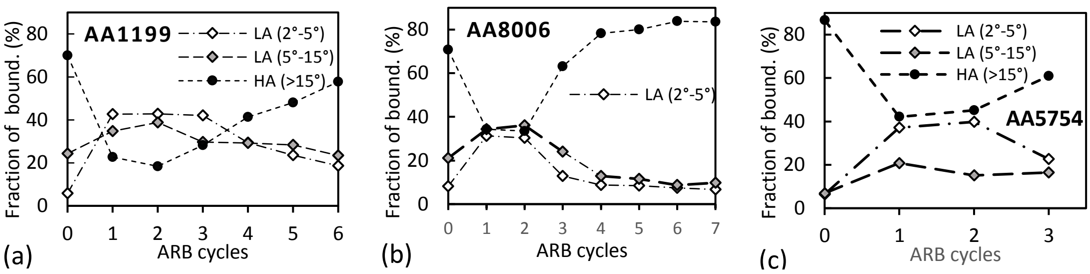

Figure 3. Evolution of fraction of low- and high-angle (sub)grain boundaries during ARB at 20°C

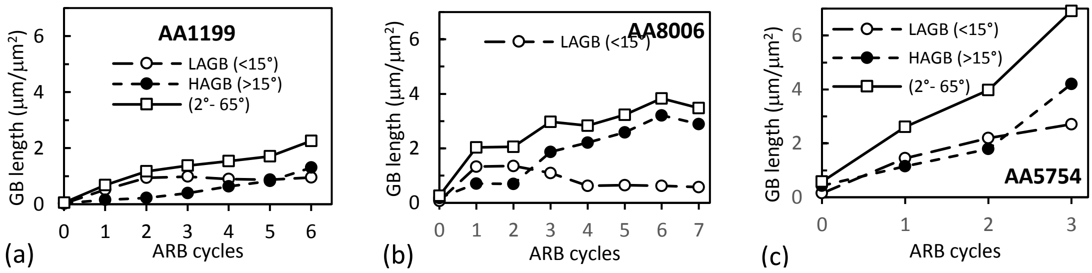

Figure 4. Evolution of specific length of low- and high-angle (sub)grain boundaries during ARB at 20°C

From Table 2 it follows that the grain size in the ND of the AA1199 and AA8006 attains 1 μm after 3 ARB cycles, but in the case of the AA5754 alloy it is already 0.59 μm after one cycle. A complementary information is the evolution of the specific length of grain boundaries (GB), which is plotted in Figure 4. The increase of the specific length of GB is the slowest in the case of AA1199 sheet (Figure 4a), it is about double for AA8006 alloy after 6 ARB cycles (Figure 4b) and in the case of the AA5754 alloy it reaches a triple value only after 3 ARB cycles (Figure 4c).

TEM observations revealed a lamellar boundary structure in all specimens (Figure 5) typical for heavily deformed materials. Nearly equiaxed subgrains with relatively high dislocation density in the subgrain interiors were observed in AA1199 and AA8006 sheets after the 1st ARB cycle. Further cycles result in subgrain flattening, and in a decrease of dislocation density in subgrain interiors due to recovery (Figure 5 a,b). In the AA5754 alloy, with high concentration of Mg atoms in the solid solution, the extent of dynamic recovery is smaller, the lamellae are thinner and the density of dislocations in grain interiors is much higher (Figure 5c).

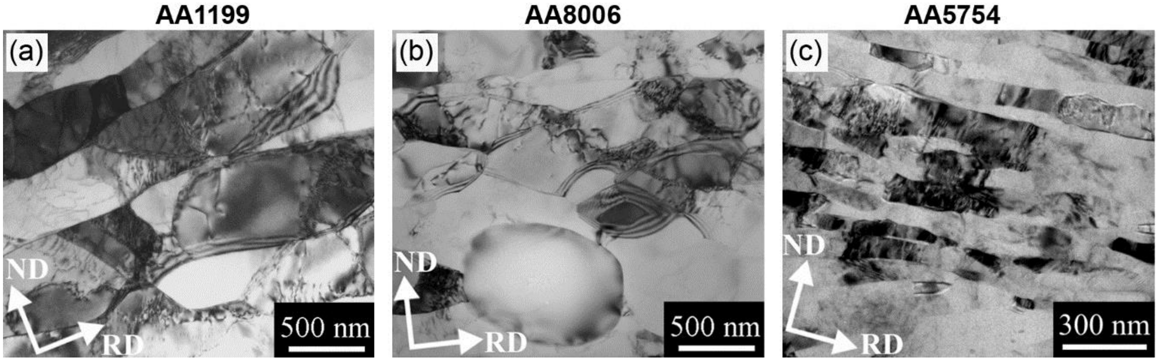

Figure 5. TEM micrographs of sheets processed at 20°C by 4 ARB cycles.

Mechanical Properties after ARB at 20°C

Hardness measurements are presented in Figure 6. All three materials show an important increase of hardness after the first ARB cycle. In the case of AA1199 and AA8006, the following cycles do not increase hardness, a slight decrease is even observed for AA1199 sheet. On the other hand, the AA5754 alloy shows a more important hardening after the first ARB cycle and the hardness continues to increase with increasing strain. The results of tensile tests are plotted in Figure 7. All materials show an important increase of the 0.2% yield stress (0.2%YS) and ultimate tensile strength (UTS) with increasing strain. The elongation decreases in an important manner after the first ARB cycle and then it remains nearly constant. In contrast to the evolution of hardness, the 0.2%YS and UTS of all materials steadily increase in the whole range of strain.

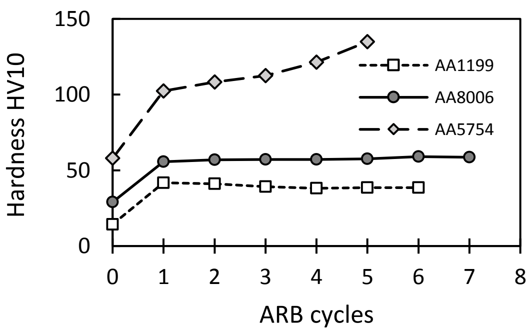

Figure 6. Hardness of sheets after ARB processing at 20°C

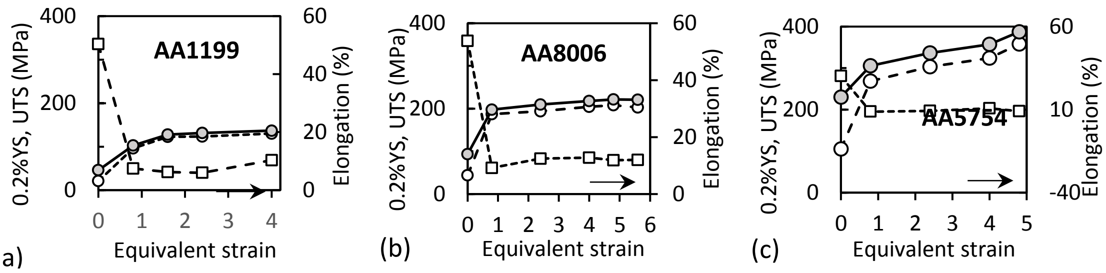

Figure 7. 0.2% yield stress (○), ultimate tensile strength (●) and elongation (□) of sheets as a function of equivalent strain induced by ARB at 20°C.

ARB of AA8006 Alloy at Elevated Temperatures

ARB processing at 200, 250, 300, and 350°C was successfully performed in the case of AA8006 and AA5754 alloys. However, the AA5754 sheet suffered from severe cracking which could not be prevented by edge trimming. Therefore, only results of AA8006 alloy are presented here. Figure 8 shows orientation maps of the AA8006 sheet after processing by 6 ARB cycles at 200, 250 and 350°C. As expected, increasing temperature of ARB processing leads to grain coarsening. If compared with the sheet processed at ambient temperature (Figure 2), the grain structure after 6 ARB cycles at 350°C (Figure 8c) and 250°C (Figure 8b) corresponds to the microstructure after 2 cycles (Figure 2e) and 3 cycles (Figure 2f) of processing at 20°C, respectively. The influence of the ARB processing temperature on the size of subgrains (LAGB) and grains (HAGB) in the ND obtained from EBSD data is summarized in Table 3. Observation in TEM after the 1st ARB cycle at 250°C revealed grains with diffuse boundaries and tangles of dislocations in their interior. But grains without dislocations or with a low density of dislocations due to dynamic recovery at elevated temperature were also found (Figure 9a). Starting from the 3rd ARB cycle, a lamellar microstructure with HAGB showing a typical fringe contrast is developed (Figure 9b,c).

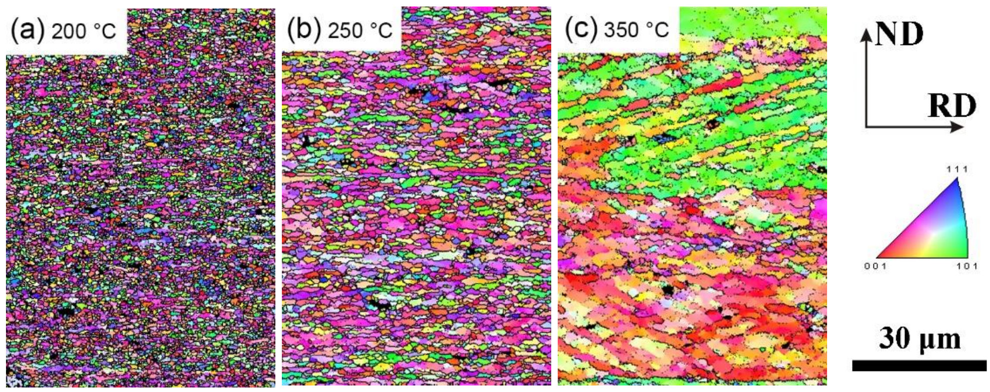

Figure 8. Orientation maps showing the grain structure of the AA8006 sheet after processing by 6 ARB cycles at elevated temperatures.

Table 3. Average distance of boundaries in the ND after 6 ARB cycles (µm, EBSD data)

Temperature of ARB (°C)	20	200	250	350
LAGB (< 5°)	0.27	0.42	0.59	0.97
HAGB (> 15°)	0.28	0.44	0.65	1.38

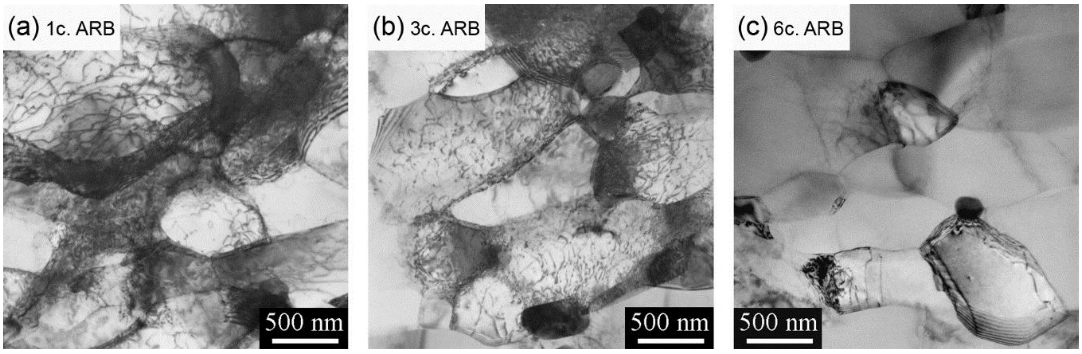

Figure 9. TEM micrographs of AA8006 sheets processed at 250°C.

Tensile Properties of AA8006 Alloy at Elevated Temperatures

The evolution of tensile properties of the AA8006 sheets as a function of processing temperature and number of ARB cycles is shown in Figure 10. As expected, the elongation is the highest at 350°C. At this temperature the strength increases only in the first ARB cycle and further ARB processing leads to the softening of the material. At 250°C the strength increases somewhat higher up to the 3rd cycle and the material also softens during further cycles, while the elongation remains almost the same (~ 12%). ARB processing at 200°C followed by a quench into ice water leads to a steady increase of strength while the elongation remains constant after the 1st ARB cycle at a comparable value. The highest and steady hardening is achieved at ambient temperature. Similarly, as at other temperatures, the elongation decreases after the first ARB cycle and then remains almost constant during further ARB processing. The elongation of the material processed at ambient temperature is comparable to that measured at 200 and 250°C.

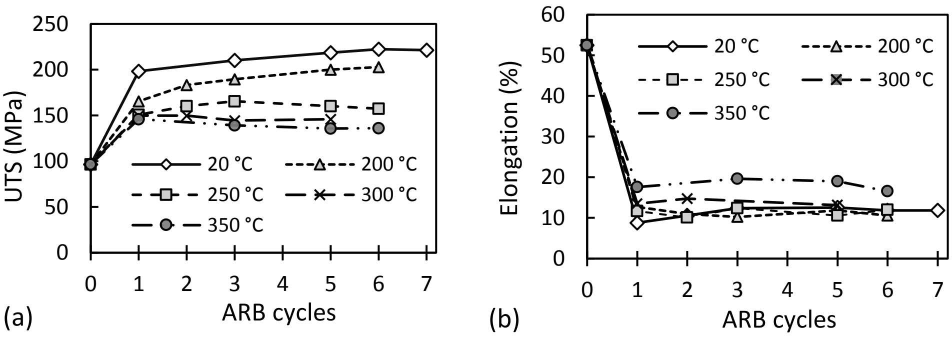

Figure 10. Ultimate tensile strength (a) and elongation (b) of AA8006 sheets ARB processed at different temperatures

CONCLUSIONS

Aluminum sheets (AA1199, AA8006, and AA5754) were processed by accumulative roll-bonding (ARB) in the temperature range from 20 to 350°C. The main results of their characterization can be summarized as follows:

i) ARB processing leads to significant grain refinement of all studied materials. The evolution of the grain structure in the first two ARB cycles is similar: LAGB formed inside grains separate cells or subgrains and deformation and shear bands appear, while the fraction of HAGB remains constant.

ii) After the 3rd ARB cycle, the fraction of HAGB in AAA1199 sheet increases moderately due to recovery. Instead, in the AA8006 and AA5754 alloys, the fraction of HAGB increases in an important manner.

iii) After processing at ambient temperature, all three materials show an important increase of hardness after the first ARB cycle. In the case of AA1199 and AA8006, the following cycles do not increase hardness, a slight decrease is even observed for AA1199 sheet.
iv) In contrast to hardness, 0.2%YS and UTS of all materials increase in the whole strain range. The elongation decreases significantly after the first ARB cycle and then it remains nearly constant.
v) ARB processing at 200, 250, 300, and 350°C was successfully performed with AA8006 and AA5754 alloys. However, the AA5754 sheet suffered from severe cracking.
vi) ARB processing of the AA8006 alloy at 200°C followed by quenching into ice water leads to a steady increase of strength with ARB cycles. At higher temperatures, the strength increase in the 1st ARB cycle is followed by softening during further cycles.

ACKNOWLEDGMENTS

This research was financially supported by ERDF (project No. CZ.02.1.01/0.0/0.0/15_003/0000485), and in part by the Czech Science Foundation (project 14-36566G). The experimental material was kindly supplied by AL INVEST Břidličná, Czech Republic.

REFERENCES

Kim, H.W., Kang, S.B., Tsuji, N., & Minamino, Y. (2005). Deformation Textures of AA8011 Aluminum Alloy Sheets Severely Deformed by Accumulative Roll Bonding, *Metallurgical and Materials Transactions A*, 36(11), 3151–3163. https://doi.org/10.1007/s11661-005-0086-3

Qu, P., Zhou, L., Xu, H. & Acoff, V. L. (2014). Microtexture Development of Niobium in a Multilayered Ti/Al/Nb Composite Produced by Accumulative Roll Bonding, *Metallurgical and Materials Transactions A*, 45(13), 6217–6230. https://doi.org/10.1007/s11661-014-2545-1

Richert, M., Liu, Q., & Hansen, N. (1999). Microstructural evolution over a large strain range in aluminium deformed by cyclic-extrusion–compression. *Materials Science and Engineering: A*, 260(1-2), 275–283. https://doi.org/10.1016/S0921-5093(98)00988-5

Roy, S., Satyaveer Singh, D., Suwas, S., Kumar, S., & Chattopadhyay, K. (2011), Microstructure and texture evolution during accumulative roll bonding of aluminum alloy AA5086, *Materials Science and Engineering: A*, 528(29-30), 8469–8478. https://doi.org/10.1016/j.msea.2011.07.042

Saito, Y., Utsunomiya, H., Tsuji, N., & Sakai, T. (1999). Novel ultra-high straining process for bulk materials—development of the accumulative roll-bonding (ARB) process. *Acta Materialia*, 47(2), 579–583. https://doi.org/10.1016/S1359-6454(98)00365-6

Tsuji, N. (2005). Production of Bulk Nanostructured Metals by Accumulative Roll Bonding (ARB) Process. In: Altan, B.S. (Ed.), Severe Plastic Deformation, Toward Bulk Production of Nanostructured Materials, Nova Science Publishers, New York, 545–565. ISBN 1-59454-508-1.

Valiev, R. Z., & Langdon, T. G. (2006). Principles of equal-channel angular pressing as a processing tool for grain refinement. *Progress in Materials Science* 51, 881–981. https://doi:10.1016/j.pmatsci.2006.02.003

Valiev, R. Z., Islamgaliev, R.K., & Alexandrov, I.V. (2000). Bulk nanostructured materials from severe plastic deformation, Progress in Materials Science, 45(2), 103–189. https://doi.org/10.1016/S0079-6425(99)00007-9

Wu, K., Chang, H., Maawad, E., Gan, W.M., Brokmeier, H.G., & Zheng, M.Y. (2010). Microstructure and mechanical properties of the Mg/Al laminated composite fabricated by accumulative roll bonding (ARB), *Materials Science and Engineering: A*, 527(13–14) 3073–3078. https://doi.org/10.1016/j.msea.2010.02.001

Xie, H., Wang, M. P., Chen, W., Jia, Y. (2016). Microstructure, Mechanical Properties, and Texture Evolution of Aluminum Alloy 7005 by Accumulative Roll Bonding, *Journal of Materials Engineering and Performance*, 25(3), 1199–1210. https://doi.org/10.1007/s11665-016-1939-1